DEVELOPMENT OF STRONTIUM FERRITE/POLYAMIDE 12 AND NEODYMIUM IRON BORON/POLYAMIDE 12 COMPOSITES USING ADDITIVE MANUFACTURING

Camila Belduque[a], Jitendra S. Tate[*,a,b], Tanjina N. Ahmed[b], Rahul Sheley[b], Wilhelmus J. Geerts[b,c], and Danny Luna[b]

Texas State University
601 University Drive, San Marcos, TX, 78666
[a]Ingram School of Engineering
[b]Materials Science, Engineering, and Commercialization Program
[c]Department of Physics
*Corresponding author: JT31@txstate.edu; Phone: 512-245-1826; Fax: 512-245-7771

ABSTRACT

Polymer matrix composite materials with magnetic properties obtained by the addition of micron-size particles of neodymium iron boron (NdFeB) and strontium ferrite for fused filament fabrication (FFF) are becoming attractive because of their potential applications in the health and automotive industries. Additionally, the design flexibility and low cost of additive manufacturing processes encourage the scientific community to create the materials and understand the properties of the parts obtained with such methods. For example, the micron-size particles of NdFeB and two different types of strontium ferrites, OP-56 and OP-71, were dispersed in the Polyamide 12 matrix using twin screw extrusion. The monofilaments produced on twin screw extrusion were used to print test samples using an open-source FFF 3D printer. Thermal analysis shows a heat flow improvement in the composites compared to neat polyamide 12. Flexural and tensile strengths of the NdFeB/PA12 and OP-71/PA12 composites were reduced, whereas OP-56/PA12 composites showed an improvement of 6% compared to neat PA12. On the other hand, the tensile moduli of OP-71/PA12, OP-56/PA12, and NdFeB/PA12 composites increased by 5.5%, 48.9%, and 25.13%, respectively.

Keywords
Polymer-matrix composites (PMCs)**,** magnetic anisotropy, twin screw extrusion, strontium ferrite, neodymium iron boron (NdFeB), additive manufacturing, fused filament fabrication (FFF).

1. Introduction

Polymer matrix composites (PMCs) are materials consisting of a polymer matrix reinforced with fibers or particles, offering superior strength, stiffness, and lightweight properties compared to traditional materials [1]. PMCs can be tailored for specific applications by adjusting their composition and processing methods [2]. Polymer matrix composites are increasingly replacing traditional material systems in aerospace, wind energy, automotive, and marine applications. Their high specific strength and modulus make them attractive to replace metallic parts. Polymer matrices, including thermoplastics and thermosets, can be modified using micro- and nanofillers to improve thermal, electrical, magnetic, and chemical properties.

One of the main advantages of these materials is their compatibility with additive manufacturing (AM) processes [3]. To the list of materials that both the AM and polymer composites industries share, bonded neodymium (NdFeB) and strontium ferrite ($SrFe_{12}O_{19}$) magnets are on the top. Although the parts obtained through these methods exhibit a lower maximum energy product and lower operational temperature compared with fully dense sintered magnets, their mechanical properties are outstanding at room temperature (RT) applications, electrical resistivity is improved, lowering eddy current losses if used in AC applications, their magnetic output can be tailored for a given size and/or shape, and the structure designs can be complex given the flexibility of the binder.

Additive manufacturing (AM) of polymer composites offers several advantages over conventional methods, including cost-effectiveness, reduced material waste, and the ability to fabricate complex geometries

[4]. Fused filament fabrication (FFF), a popular AM technique, allows for control over filler alignment and orientation, enabling tailored mechanical, thermal, and electrical properties [5]. Recent advancements in additive manufacturing of polymer composites emphasize the integration of fillers to enhance mechanical properties, optimize filler alignment, and enable multi-scale material design for improved functionalities [6]. AM of polymer composites addresses the limitations of pure polymer components, such as poor strength and functionality [7]. The technology finds applications in various industries, including biomedical, automotive, and aerospace [8]. The addition of $SrFe_{12}O_{19}$ to NdFeB composites can improve thermal stability but may decrease overall magnetic performance [9]. Particle alignment during printing can significantly enhance magnetic properties, with remanence increases of up to 40% reported for anisotropic structures [10]. Particle orientation and axial diameter ratio significantly influence the magnetic permeability of anisotropic soft magnetic composites, with optimal alignment enhancing permeability [11]. However, challenges remain, such as optimizing print quality and expanding available materials [12]. Recycling strategies are crucial for improving the sustainability of polymer composite AM, particularly in FFF, where thermoplastic-based feedstocks are highly amenable to recycling [13]. Particle-binder debonding and decreased thermal stability require further investigation [14].

Neodymium (NdFeB) is an intermetallic compound, classified as a permanent/hard magnet; this property highly depends on the microstructure of the manufacturing process. Their capacity to generate a strong magnetic field in a small volume (512 kJ/m^3), availability, and recyclability place them as the world's most acquired type of magnets, given the increasing demand for renewable energy sources, electric vehicles and electronics. Some of its drawbacks are its low curie temperature (T_c), which goes around 311°C, brittleness, sensitivity to corrosion, and high cost. NdFeB magnets are being actively investigated using different AM processes. For instance, Huber et al., 2020 [15] manufactured magnets through stereolithography (SLA), selective laser sintering (SLS), and fused filament fabrication (FFF) to compare the magnetic properties of NdFeB composites and surface finish obtained through each method. The SLA results are the most promising for the latter, whereas FFF seems to yield a higher roughness to the structure, and SLS parts show a more brittle behavior. The remanence of the SLS samples is higher than that of the FFF and SLA samples. In contrast, its coercivity is lower than FFF, SLA's samples yield better, and almost equal values are attributed to grain size and distribution uniformity. These properties are influenced by melting and rapid cooling. They can be improved by preventing complete melting of the material—specifically, through sintering—which facilitates better microstructure control. Laser additive manufacturing (LAM) offers high flexibility and stability for complex structures but introduces challenges such as high-temperature gradients, porosity, and coarse columnar grains [16]. In-situ field-assisted techniques, including ultrasound and magnetic fields, have been explored to refine, melt pool morphology and grain nucleation, improving part quality [16].

Strontium ferrite ($SrFe_{12}O_{19}$), barium ferrite ($BaFe_{12}O_{19}$,) and cobalt ferrite ($CoFe_2O_4$) powders are also becoming highly employed for AM. These particles are obtained through powder metallurgical methods and yield lower magnetic moment densities of iron and rare earth magnets. Outstanding magnetic properties are not the only characteristics studied in polymer composites filled with ferrites. For instance, Hanemann et al., 2020 [17] investigated the mechanical properties of barium ferrites and acrylonitrile butadiene styrene (ABS). They obtained a reduction in the tensile strength, ultimate stress, and ultimate strain of such composites at different loading levels. The results were attributed to the fillers creating discontinuities and poor 3D printing quality causing voids. Additionally, the material's magnetic behavior decreased. In polymer composites, it is crucial to guarantee a good adhesion that allows fillers to support most of the applied load before transferring it to the matrix. The filler/matrix adhesion depends on the chemical characteristics of both components and can be improved with surface modifiers in some cases [18].

Additionally, the extruder, which is used to produce the filaments for FFF, highly influences the filament quality in terms of voids. For example, twin-screw extruders have two co-rotating screws that improve the dispersion and the shear in the polymer during the different thermal stages from the cooling zone to the die. Additionally, they include vacuum systems designed to eliminate trapped air and other gaseous contaminants. Unlike typical single-screw extruders, which lack vacuum systems, the low shear induced by the screw limits both the types of materials that can be manufactured and their quality [19]. In another paper, Huber et al.,

2020 [20] investigated the mechanical and magnetic properties of strontium ferrite/PA12 composites; they found a decrease in the tensile strength as the filler content (up to 55 vol%) increased. However, the tensile strain at break increased considerably.

Currently, literature on the magnetic behavior of 3D-printed hard magnetic material is scarce. Furthermore, only two magnetic filaments are commercially available: Iron/PLA by Protopasta and Iron/PLA by Black Magic. Mechanically, such material shows a brittle behavior, which complicates the 3D printing process [21].

The main goal of this study is to manufacture NdFeB/PA12 filaments, and two types of $SrFe_{12}O_{19}$ filament composites, namely OP-71/PA12 and OP-56/PA12, for fused filament fabrication (FFF) purposes by using a co-rotating twin screw extruder. A study by Mehrifar et.al. [22] explains the NdFeB nanoparticles synthesized via wet ball milling exhibit enhanced ferromagnetic properties and thermal stability, with particle size reduction significantly influencing magnetic performance. Single-screw extruder led to agglomeration and could not provide sufficient shear forces to effectively distribute the high filler content, leading to inconsistent filament properties. Twin screw provides superior dispersion, precise thermal control reducing the risk of degradation. FFF is selected due to its lower capital costs compared to SLS and SLA. The materials and processes used in FFF are widely available, making it accessible to industry, academia, and home users. Most importantly, FFF can be adapted to print anisotropic magnets, which offer higher remanence and energy products than isotropic magnets at the same loading level. The shape, size, and distribution of the magnetic particles within the matrix are analyzed using a JEOL Scanning Electron Microscope. An SDT 650 performs Thermogravimetric Analysis (TGA) and Differential Scanning Calorimetry (DSC). Lastly, the flexural and tensile behavior of 3D-printed samples is evaluated according to ASTM D790 and D638, respectively.

2. Experimentation

2.1. Material System

The filaments are manufactured using the same polymer matrix and three different types of magnetic particles. Vestosint 3D Z2773 Nylon 12 is chosen as the polymer matrix due to high flowability, chemical stability and good adhesion properties for uniform magnetic dispersion; it is a powder obtained from Evonik with high flowability and chemical stability, which indicates an excellent capacity to be mixed with other materials and provide good adhesion. Additionally, it has low moisture absorption compared to other polyamides. The magnetic particles used are strontium ferrite OP-71 and OP-56 ceramic-based hard magnetic materials known for their coercivity and stability under high temperature from DOWA Electronics Inc, to fill the PA12 at a 50 wt%. Table 1 includes the main properties of these particles given by the manufacturer.

Table 1. Material properties of OP-71 and OP-56 strontium ferrite particles.

$SrFe_{12}O_6$	Remanence [emu/cm^3]	Coercivity [Oe]	Density [g/cm^3]	Particle Size [µm]
OP-71	151	2510.7	3.33	1.5-2.5
OP-56	152	3091.3	3.09	1.01

The third filament composite is filled with NdFeB at a 50wt%, obtained from Nanochemazone Inc; these particles range from 5 to 10 µm provided by the manufacturer.

2.2. Manufacturing

Both constituents were mixed in a centrifugal planetary mixer (THINKY™ ARV-310) to improve the mixing of the fillers in the PA12. A filler concentration of 50wt% for each composite is mixed at 500 rpm. The mixing process involves five cycles, followed by a three-minute resting period, and no vacuum is applied.

To generate shear, twenty ceramic balls, each with a diameter of 10 mm, are added to the container. These specific parameters were chosen to prevent long mixing times, which could potentially grind the magnetic particles and alter the magnetic properties of the composites.

Process 11 Twin Screw Extruder produced magnetic particles filled PA 12 composite filaments. It has nine temperature zones to gradually melt, mix, and extrude the materials. The vacuum was applied during stage seven. The temperatures for all composites were set as follows: z_1: cool zone, z_2: 220°C, z_3: 230°C, z_4: 230°C, z_5: 240°C, z_6:240°C, z_7:240°C, z_8:230°C, and die: 220°C. This temperature range allowed the composite material to flow continuously. Neat PA12 was extruded with the highest temperature at 220°C to avoid thermal degradation. Although the exact temperature was targeted for producing the composites, the material's viscosity was too high, causing the torque in the extruder to exceed the allowed limit.

Consequently, the temperature on the twin-screw extruder was increased to the above values to avoid high torque on the machine and obtain a continuous filament. During this process, the screw speed was synchronized with the spooler speed to prevent excessive reduction in the diameter of the composite as it leaves the die. Note that this process also facilitated the obtention of the desired filament diameter, 1.75 mm, by allowing more material to accumulate in the barrel, generating the correct pressure for extrusion. The cooling method consisted of a water bath placed under the die; two guides decreased the filament waving-like movement in the water. Also, when guides touched the filament, it ensured it wasn't pulled down the die, preventing the diameter reduction. Both OP-71/PA12 and OP-56/PA12 filaments required us to modify different parameters during the process to obtain a 1.75 mm diameter. NdFeB/PA12 was more straightforward to process in this aspect. Nevertheless, twin-screw extruders are known for yielding varying filament diameters. This issue is commonly solved by pelletizing the material and extruding it with a single-screw extruder or upgrading the machine with a melt pump [23].

Although the average diameter of the NdFeB/PA12 filament was easier to control, one difficulty during the extrusion of this material was the fluctuation in pressure that would induce sudden diameter variations of up to 0.3 mm. However, Ponsar et al., 2020 attributed this to the accumulation of material in the die, which leads to changes in pressure and die swell, as shown in our case in Fig. 1 below [24].

Figure 1. Die swell in NdFeB/PA12 filament after extrusion.

2.3. Fused Filament Fabrication

A CrafBot XL3 was used to print type I samples needed for ASTM D638 for tension testing, targeting a thickness of 3.25 mm. The samples were printed in zero magnetic fields. The first printed sample had a thickness 0.4 mm larger than the designed one. Therefore, the CAD file adjusted the thickness to compensate for such an increment. Flexure properties were evaluated following the ASTM D790 standard. The flexural sample size was 70 mm long x 12.7 mm wide x 3.25 mm thick, as specified by the ASTM for cases where the nose and support rollers have a radius different than 5 mm. The G-codes for both tensile and flexure tests were used to print all layers in the same direction, parallel to the longitudinal direction, and with a 100% infill density. The 3D printing was carried out using a 0.4 mm hardened steel nozzle and a layer thickness of 0.2

mm. The nozzle temperature of 235°C was tried in the beginning to ensure a decrease in thermal stresses, but printing was obstructed several times. Therefore, the nozzle temperature gradually increased up to 260°C, the optimum value at which all the composites could be printed with no difficulties. Additionally, metallic and glass beds heated at 95°C were used to deposit specimens. However, the first layers did not attach to the bed properly and were pushed out of the platform by the nozzle. Therefore, the fans were turned off, and glue and paper were needed to guarantee adhesion of the first two layers to the bed, which were printed at 50% speed, 30 mm/sec.

The NdFeB/PA12 samples were successfully printed without any modification to the 3D printer because of the brittle nature of the filler, which decreased the flexibility of the composite. Nevertheless, both OP-71/PA12 and OP-56/PA12 composites required the drive gears to be adjusted in the filament feed section to avoid buckling due to the nylon's flexibility, as observed in Figure 2. The filament buckling was avoided by increasing the height of the filament guide and adding a different mount able to contain the filament.

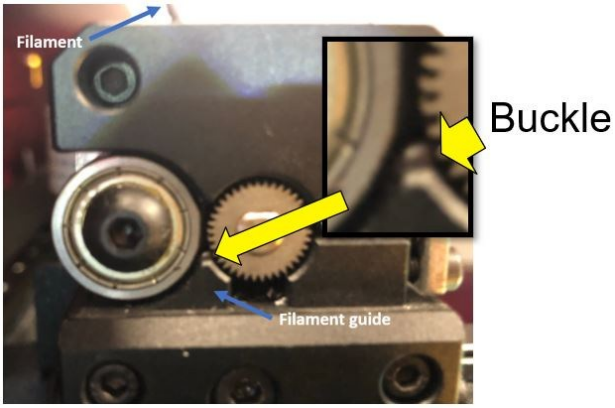

Figure 2. CraftBot XL3 feeding zone and OP-56/PA12 filament buckling between the drive gears.

3. Characterization and results

3.1. Density Measurements

The density of both the composites and neat PA12 was obtained following the ASTM D792-20. A cylinder 5 mm high and 20 mm in radius was printed as the standard requires at least two samples of each material with a volume higher than 1 cm^3 and soft edges. The method consists of weighing the specimen in air and demineralized water to find the specific gravity and density. The values below are the averages obtained from the two samples tested.

Table 2. Density values of neat PA12 and composites with 50 wt% filler loading (ASTM D792).

Density [g/cm^3]			
PA12	**NdFeB/PA12**	**OP-56/PA12**	**OP-71/PA12**
1.04	1.62	1.60	1.40

3.2. Scanning Electron Microscope (SEM)

A JEOL JSM-6010 PLUS/LA SEM was used to observe the different powders, composites, and 3D-printed specimens to understand how the alignment and distribution of the particles change when they are printed with or without a magnetic field. All samples were coated with a 2 nm layer of gold deposited by a Quorum Technologies EMS150T Imaging Sputter Coater. to avoid charging effects. In Figure 3, it is observed that the NdFeB particles do not have a specific shape. The NdFeB particle range size varies from 0.5 µm to as large as 15 µm. OP-51 and OP-56 showed smaller plate-like particles between 0.25 – 4 µm. In

magnetic materials, the coercivity increases as the particle size decreases to the single domain size limit [25]. For permanent magnets, minor variations in size are preferred to obtain constant magnetic properties in filled polymers. Moreover, particle size distribution may also influence how the composites support the flexure and tension load because large particles tend to form clusters, as will be seen in the SEM images obtained, which can lead to large spaces without particles that serve to transfer the mechanical loads and increase the resistance of the polymer.

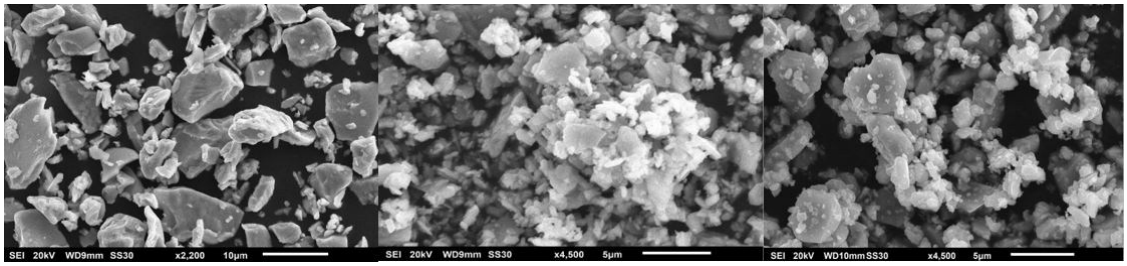

Figure 3. SEM images of left to write (a)NdFeB, (b) OP-56, and (c) OP-71 in powder form.

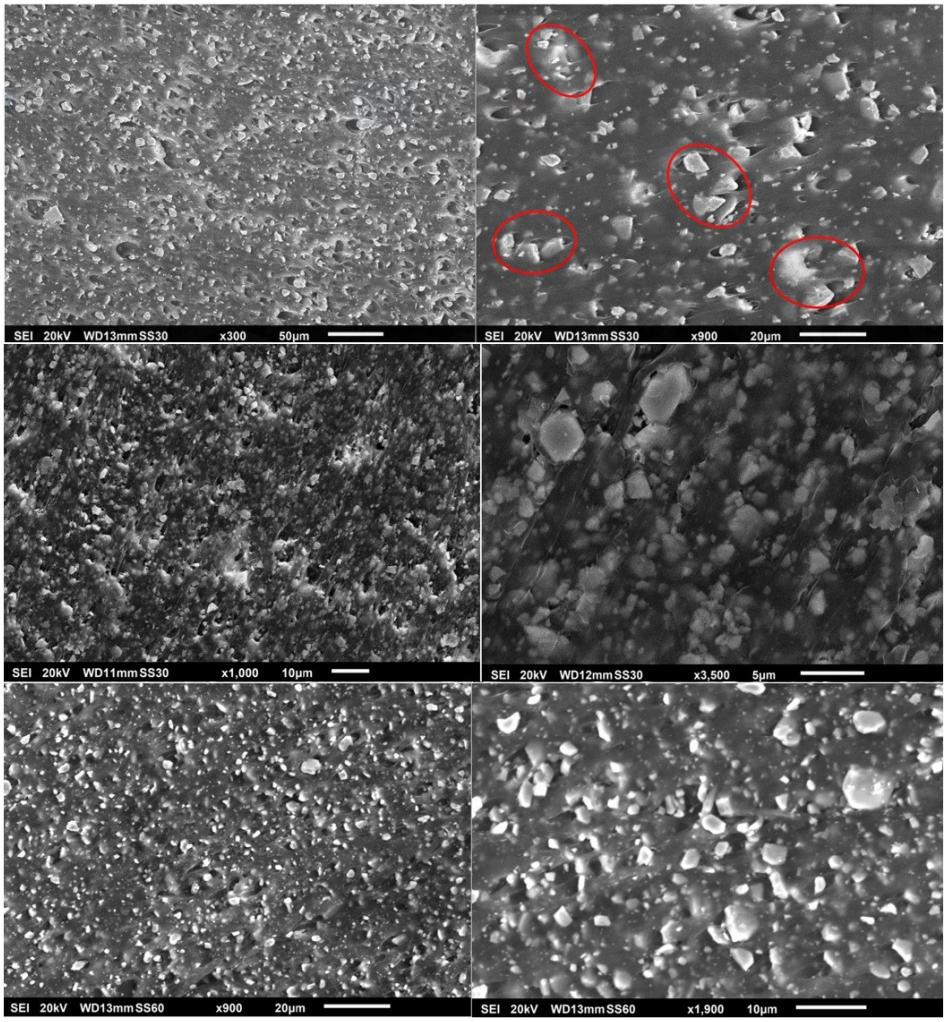

Figure 4. SEM images of composite filaments: (a) NdFeB/PA12 (top), (b) OP-56/PA12 (middle), and (c) OP-71/PA12 (bottom).

Three random samples of each filament were chosen, and SEM images were taken at different locations to analyze the distribution of the particles in PA12. In Figure 4, the first two images show the distribution of the particles in the NdFeB/PA12 filament, in which large particles seem to be close to each other because of their stronger magnetic dipole interaction, while smaller particles are better dispersed. The distribution between particles is more homogeneous for the OP-71/P12 and OP-56/PA12 filaments shown in the middle and third row of the same figure. No apparent clustering of larger particles was observed, like the NdFeB composite. Moreover, the OP-56 powders appear to have a morphological alignment obtained during extrusion in a zero magnetic field, which could result in anisotropic magnetic properties. However, chaining of magnetic particles has been observed by other scientists[26, 27] in low viscous suspension, including $SrFe_{12}O_{19}$/PDMS[19], and the higher viscosity of the molten $SrFe_{12}O_{19}$/PA12. The elevated temperature lowers magnetostatic interaction, making sole chaining less likely for these composites. The observed alignment for the OP-56/PA12 filament might be partly because of flow during the extrusion process on the orientation of plate-like particles.

3.3. Thermogravimetric Analysis and Differential Scanning Calorimetry

TA Instruments' SDT 650 Thermal Analyzer was used to perform TGA and DSC analyses on the composites and neat PA12. All tests were ramped with a heating rate of 20°C/min up to 600°C in a nitrogen environment. Figure 5 displays the TGA overlay of neat PA12 and other composites. The polymer loses weight in two stages, from 290.4°C to 370°C by 1.69%. From that point on, the decomposition occurs faster, leaving a remaining of less than 2% at 588°C. All composites start degrading at around 409°C, a stage at which they have decreased 1.4% in average weight compared with 4.8% of neat PA12, indicating a slight improvement in heat transfer between the matrix and magnetic fillers because of more significant thermal conductivity of the latter during the first degradation stage that delays the decomposition of the material. Strontium ferrite has been shown to exhibit thermal anisotropy, transferring heat more efficiently in the in-plane direction than in the cross-section direction [28].

Figure 6 depicts the DSC measurements; a slightly pronounced endothermal corresponding to the glass transition temperature (Tg) appears at 77.9°C, 61.7°C, and 64.2°C for the OP-71, OP-56, and NdFeB composites, respectively. Neat PA12 registers a value of 68.8°C. All curves slightly increase towards the crystallization temperature (Tc) at around 123°C and a second endothermic appears, indicating melting temperature (Tm) at 188.5°C, 184.5°C, 184 °C for OP-71, OP-56, and NdFeB composites, neat PA12 shows a similar value of 188.5°C that significantly continues decreasing until 456.4°C before abruptly increasing again. This may be due to the decrease in thermal stability at this temperature, where the sample has lost 63% of its weight. Similar values have been reported in other studies [29]. OP-56/PA12 starts decomposing faster, reaching a 48% weight loss in the range of 452.7°C to 503°C. The 52% remaining weight corresponds to the filler and the beginning of forming different iron and strontium oxide phases. A similar behavior is observed with OP-71/PA12, which loses 5% more weight than OP-56/PA12 at 503°C. The lower high-temperature weight is consistent with the density data in Table 1. Figure 5 shows that the strontium composites have better stability than NdFeB/PA12, whose first decomposition stage is observed to be between 413°C and 453°C. This point marks the beginning of a faster weight loss that reaches 45% with a temperature increase. The augment emerging from 453°C to 588°C is attributed to corrosion attack, which gives place to oxides such as Fe (II) (FeO) and Fe (III) (Fe_2O_3), Nd_2O_3 , and α-Fe_2O_3 [14]. Extrapolation of the high-temperature slope to the 50 wt% level suggests that NdFeB oxidation starts at 400ºC. Table 3 summarizes these results.

Table 3. Thermal properties of neat PA12 and composites

Material	T_g [°C]	T_c [°C]	T_m[°C]
Neat PA12	68.8	122.9	188.5
OP-71/PA12	77.9	120.9	188.5
OP-56/PA12	61.7	125.6	184.5
NdFeB/PA12	64.2	126.32	184.05

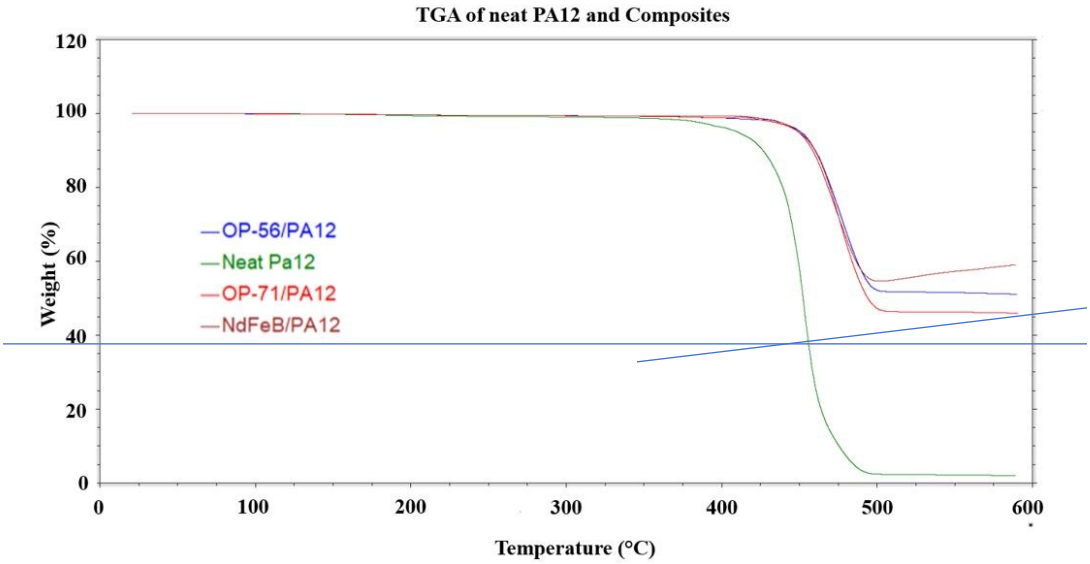

Figure 5. Thermogravimetric Analysis **(**TGA) results of neat PA12 and composites with a 50wt% filler loading.

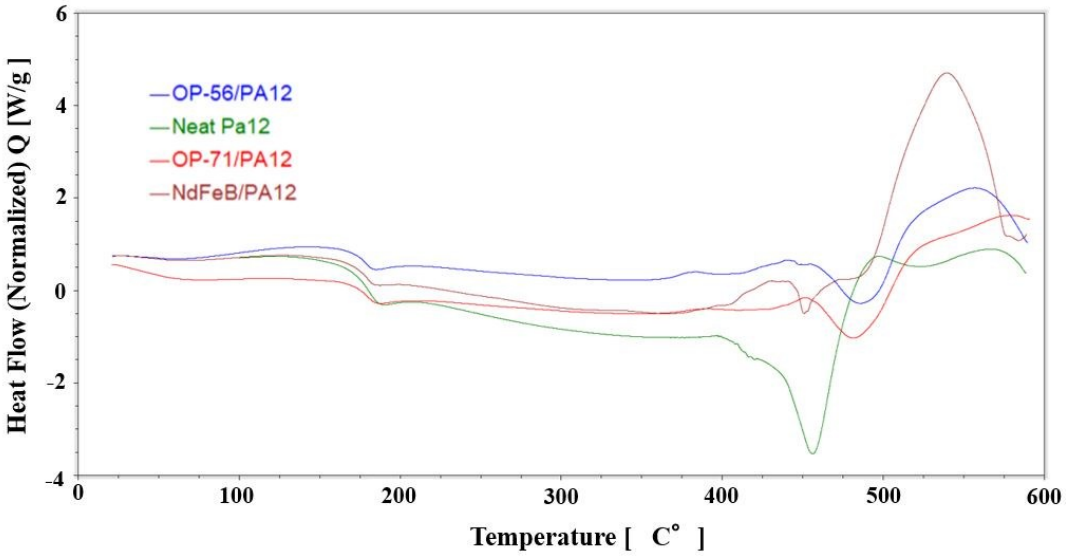

Figure 6. Differential Scanning Calorimetry (DSC) results of neat PA12 and composites with 50 wt% filler loading.

3.4. Mechanical Properties

Five samples of each composite system and neat PA12 were tested under flexure and tension using Servo-hydraulic Material Testing System 810 following ASTM D790 and ASTM D638, respectively. There is a minimal decrease in the flexural strength of PA12 when it is loaded with 50wt% of $SrFe_{12}O_{19}$ and NdFeB, and the flexural modulus of OP-56 increases by 7%. In previous studies, at 40wt% of $SrFe_{12}O_{19}$/PA12 these properties increased by 18% and 30%, respectively. This can be attributed to the polymer's different thermal stresses during extrusion and 3D printing. For instance, at 40wt%, the OP-71/PA12 could be printed at 235°C, while the current loading level requires 35°C more to avoid nozzle obstructions [30]. This temperature is

considered high given that the PA12 decomposition point starts at around 300°C, according to the manufacturer, and confirmed in in-house TGA results. Additionally, during 3D printing, the particles could reorganize in the polymer as it was melting and passing through the nozzle, producing a non-homogeneous distribution and, consequently, affecting mechanical properties (Figure 7).

The failure modes of composites and neat PA12 under tensile loading are illustrated in Figure 8. Although none of the samples failed inside the grip area, not all ruptures are entirely in the middle zone.

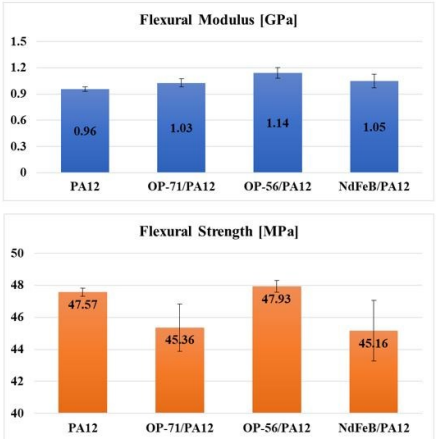

Figure 7. Flexural modulus (GPa) and flexural strength (Mpa) values of composites manufactured at 50wt% loading levels.

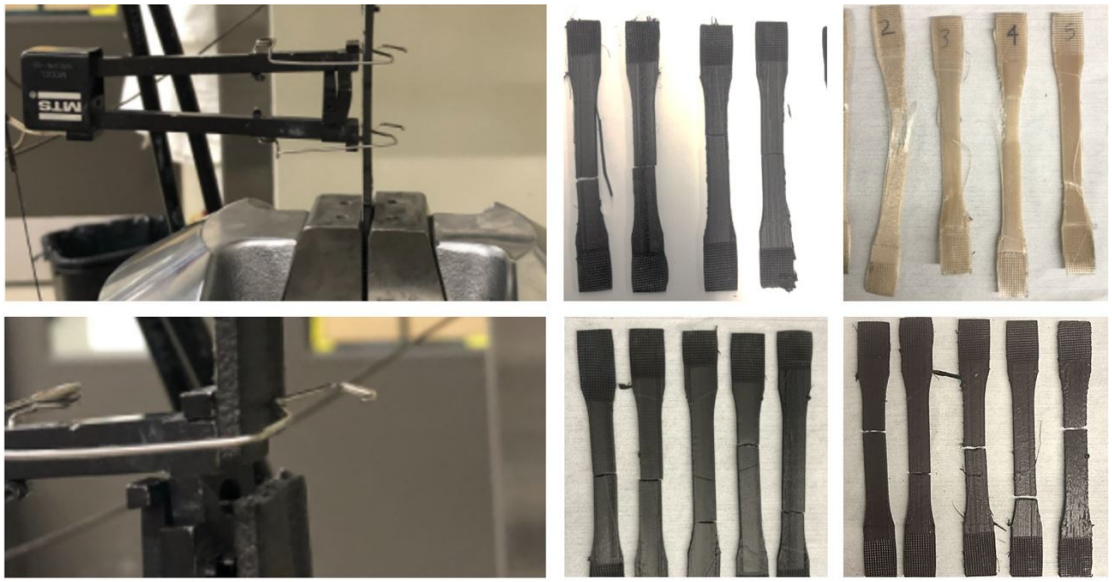

Figure 8. Tensile test setting and tested samples of OP-71/PA12, PA12, NdFeB/PA12, and OP-56/PA12 composites.

The tensile modulus of OP-71/PA12, OP-56/PA12 and NdFeB/PA12 increases by 5.5%, 48.9% and 25.13%, respectively compared to neat PA12. Therefore, the ability of these materials to withstand higher loads is enhanced before they reach the plastic zone. After the elastic zone, the composites exhibit brittle behavior, while the neat PA12 shows signs of necking. This explains why there are no significant changes in tensile strength, with OP-56/PA12 being the only composite that shows a slight increase of 6%. The actual

impact of this load is illustrated in Figure 9, which also displays the failure modes of both neat PA12 and composites.

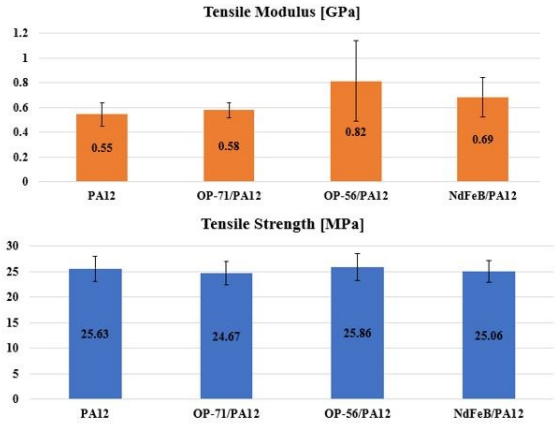

Figure 9. Ultimate Tensile strength (MPa) and tensile modulus (GPa) of neat PA12 and composites.

4. Conclusions

Magnetic filament composites were successfully manufactured using twin screw extrusion. 50wt% of two conventional magnetic materials, $SrFe_{12}O_{19}$ and NdFeB, were added to a Nylon 12 matrix. The temperature range required to obtain the mentioned composites is higher than that of the control material due to the rheology changes when reinforcements are added. The settings of extruder screws and the feeder's rpm need to be optimized to eliminate the die swell in the NdFeB/PA12 filaments and increase the diameter of the $SrFe_{12}O_{19}$/PA12 filaments. TGA and DSC analyses performed on all the materials show an improved heat flow in the composites compared to the neat PA12. Additionally, all the composites show an increase in weight% due probably to the formation of oxides when the magnetic particles reach around 500°C.

Samples for mechanical tests were obtained using a commercial 3D printer requiring a hardened steel nozzle of 0.4 mm. The buckling effect, common in flexible filaments, represented a challenge during the 3D printing of both OP-71 and OP-56-based composites and required the 3D printer to be upgraded. This should be improved by increasing the filament loading level, resulting in more rigid material being pushed down more easily by the 3D printer rollers. All composites show a higher tensile modulus; NdFeB/PA12, OP-56/PA12, and OP-71/PA12 increased by 5.5%, 48.9% and 25.13%, respectively. The flexural strength is only improved by 6% in NdFeB/PA12 composites. Additionally, the flexural modulus increased by 7.5%, 19.6% and 9.8% for OP-71/PA12, OP-56/PA12 and NdFeB/PA12, respectively

5. Acknowledgments

This paper's authors are thankful to the Advanced Composites Laboratory researchers and Ruben Villareal from Texas State University for their contribution to this project with their time and technical skills. We also want to thank the Maker Space staff at Texas State University for facilitating the 3D printers. The work was partly supported by NSF through a DMR-MRI Grant under Awards 1726970 and 2216440, partly by DOD through an HBCU/MI grant (78810-W911NF2010298), and by a Research Enhancement grant from Texas State University. The authors also acknowledge support from the Graduate College of Texas State through a thesis and dissertation support grant.

REFERENCES

[1] D. Brabazon, "Introduction: Polymer Matrix Composite Materials," *Encyclopedia of Materials: Composites,* 2021.

[2] Y. Tamsilian, S. Alvani, F. Abdolkhani, and E. K. Moghadam, "Tailored Behavior of Polymer Matrix Composite Materials," *Encyclopedia of Materials: Composites,* 2021.

[3] A. El Moumen, M. Tarfaoui, and K. Lafdi, "Additive manufacturing of polymer composites: Processing and modeling approaches," *Composites Part B: Engineering,* vol. 171, pp. 166-182, 2019/08/15/ 2019, doi: https://doi.org/10.1016/j.compositesb.2019.04.029.

[4] K. Markandan and C. Lai, "Fabrication, properties and applications of polymer composites additively manufactured with filler alignment control: A review," *Composites Part B: Engineering,* 2023.

[5] K. Niendorf and B. Raeymaekers, "Additive Manufacturing of Polymer Matrix Composite Materials with Aligned or Organized Filler Material: A Review," *Advanced Engineering Materials,* vol. 23, 2021.

[6] E. Natarajan, Markandan, K., Hassan, C.S., & G. Koppad, P. , *Sustainable Structural Materials: From Fundamentals to Manufacturing, Properties and Applications (1st ed.).* , 1st Edition ed. Boca Raton: CRC Press., 2025, p. 352.

[7] R. Keshavamurthy, V. Tambrallimath, and D. Saravanabavan, "Development of Polymer Composites by Additive Manufacturing Process," 2021.

[8] S. D. Shelare, K. R. Aglawe, S. S. Giri, and S. N. Waghmare, "Additive Manufacturing of Polymer Composites: Applications, Challenges and Opportunities," *Indian Journal of Engineering and Materials Sciences,* 2023.

[9] F. Yang, X. Zhang, Z. Guo, S. Ye, Y.-l. Sui, and A. A. Volinsky, "D printing of NdFeB bonded magnets with SrFe 12 O 19 addition," 2018.

[10] C. Huber, S. Cano, I. Teliban, S. Schuschnigg, M. Groenefeld, and D. Suess, "Polymer-bonded anisotropic SrFe12O19filaments for fused filament fabrication," *Journal of Applied Physics,* 2019.

[11] S. Wu, Dong, Z., Sun, X. et al. , "Influence of Particle Orientation Angle and Axial Diameter Ratio on the Magnetic Properties of Soft Magnetic Composites by Finite Element Method.," *J Supercond* vol. Nov Magn 38, 7 2025, doi: https://doi.org/10.1007/s10948-024-06856-w.

[12] S. Park, W. Shou, L. Makatura, W. Matusik, and K. K. Fu, "3D printing of polymer composites: Materials, processes, and applications," *Matter,* 2022.

[13] A. Sola and A. Trinchi, "Recycling as a Key Enabler for Sustainable Additive Manufacturing of Polymer Composites: A Critical Perspective on Fused Filament Fabrication," *Polymers (Basel),* vol. 15, 2023.

[14] L. Pigliaru *et al.*, "3D printing of high performance polymer-bonded PEEK-NdFeB magnetic composite materials," *Functional Composite Materials,* vol. 1, no. 1, p. 4, 2020/05/19 2020, doi: 10.1186/s42252-020-00006-w.

[15] C. Huber, G. Mitteramskogler, M. Goertler, I. Teliban, M. Groenefeld, and D. Suess, "Additive Manufactured Polymer-Bonded Isotropic NdFeB Magnets by Stereolithography and Their Comparison to Fused Filament Fabricated and Selective Laser Sintered Magnets," (in eng), *Materials (Basel),* vol. 13, no. 8, p. 1916, 2020, doi: 10.3390/ma13081916.

[16] C. Chen, Z. Zhang, Y. Cai, Y. Liu, and H. Chen, "Research and development status of in situ field assisted laser additive manufacturing: A review," *Optics & Laser Technology,* vol. 181, p. 111700, 2025/02/01/ 2025, doi: https://doi.org/10.1016/j.optlastec.2024.111700.

[17] T. Hanemann, D. Syperek, and D. Nötzel, "3D Printing of ABS Barium Ferrite Composites," *Materials (1996-1944),* Article vol. 13, no. 6, p. 1481, 03/15/ 2020, doi: 10.3390/ma13061481.

[18] H. Kallagunta and J. S. Tate, "Low-velocity impact behavior of glass fiber epoxy composites modified with nanoceramic particles," *Journal of Composite Materials,* vol. 54, no. 16, pp. 2217-2228, 2020/07/01 2019, doi: 10.1177/0021998319893435.

[19] A. Shrivastava, "5 - Plastics Processing," in *Introduction to Plastics Engineering*, A. Shrivastava Ed.: William Andrew Publishing, 2018, pp. 143-177.

[20] C. Huber, S. Cano, I. Teliban, S. Schuschnigg, M. Groenefeld, and D. Suess, "Polymer-bonded anisotropic SrFe12O19 filaments for fused filament fabrication," *Journal of Applied Physics,* vol. 127, no. 6, p. 063904, 2020, doi: 10.1063/1.5139493.

[21] L. Bollig, M. Patton, G. Mowry, and B. Nelson-Cheeseman, "Effects of 3D Printed Structural Characteristics on Magnetic Properties," *IEEE Transactions on Magnetics,* vol. PP, pp. 1-1, 04/25 2017, doi: 10.1109/TMAG.2017.2698034.

[22] Y. Mehrifar, Moqtaderi, H., Hamidi, S.M. , "Magnetic nanoparticles of Nd2Fe14B prepared by ethanol-assisted wet ball milling technique. ," *Sci Rep* vol. 15, 3257 2025, doi: https://doi.org/10.1038/s41598-025-87301-3.

[23] C. Martin, "Twin Screw Extrusion for Pharmaceutical Processes," in *Melt Extrusion: Materials, Technology and Drug Product Design*, M. A. Repka, N. Langley, and J. DiNunzio Eds. New York, NY: Springer New York, 2013, pp. 47-79.

[24] H. Ponsar, R. Wiedey, and J. Quodbach, "Hot-Melt Extrusion Process Fluctuations and their Impact on Critical Quality Attributes of Filaments and 3D-printed Dosage Forms," (in eng), *Pharmaceutics,* vol. 12, no. 6, Jun 3 2020, doi: 10.3390/pharmaceutics12060511.

[25] S. Mørup, M. F. Hansen, and C. Frandsen, "1.14 - Magnetic Nanoparticles," in *Comprehensive Nanoscience and Technology*, D. L. Andrews, G. D. Scholes, and G. P. Wiederrecht Eds. Amsterdam: Academic Press, 2011, pp. 437-491.

[26] A. d. O. Barros, M. N. H. Kashem, D. Luna, W. J. Geerts, W. Li, and J. Yang, "Magnetic properties of PDMS embedded with strontium ferrite particles cured under different magnetic field configurations," *AIP Advances,* vol. 12, no. 3, p. 035121, 2022, doi: 10.1063/9.0000338.

[27] K. Butter, P. H. H. Bomans, P. M. Frederik, G. J. Vroege, and A. P. Philipse, "Direct observation of dipolar chains in iron ferrofluids by cryogenic electron microscopy," *Nature Materials,* vol. 2, no. 2, pp. 88-91, 2003/02/01 2003, doi: 10.1038/nmat811.

[28] A. D. Volodchenkov *et al.*, "Magnetic and thermal transport properties of SrFe12O19 permanent magnets with anisotropic grain structure," *Materials & Design,* vol. 125, pp. 62-68, 2017/07/05/ 2017, doi: https://doi.org/10.1016/j.matdes.2017.03.082.

[29] M. Kwiatkowska, R. Pełech, A. Jędrzejewska, D. Moszyński, and I. Pełech, "Different Approaches to Oxygen Functionalization of Multi-Walled Carbon Nanotubes and Their Effect on Mechanical and Thermal Properties of Polyamide 12 Based Composites," (in eng), *Polymers (Basel),* vol. 12, no. 2, p. 308, 2020, doi: 10.3390/polym12020308.

[30] C. Belduque *et al.* (2021) Magnetic and Mechanical Characterization of Additive Manufactured Strontium Ferrite/Polyamide 12 Composites Using Twin-Screw and Single-Screw Extrusion. *SAMPE neXus Proceedings* [Conference]. 686-697.